Chapter 13

Boundary-Multipole Collocation

13.1 Introduction

On several occasions, we mentioned the boundary-multipole collocation method as a tool for solving particle-particle hydrodynamic interaction problems. We now devote a chapter to explore this technique in depth: definition of the method, analysis of discretization errors, variations on the standard method, and last but not least, an exposition of the method as applied to interactions between particles. The emphasis will be on the applications to the calculation of resistance and mobility functions of spheres and ellipsoids.

Collocation methods are well established in the world of numerical methods as an important tool for solving boundary value problems. In the more familiar interior collocation (or simply collocation) method, the trial solution is expanded in a set of basis functions that trivially satisfy the boundary conditions, but not the governing differential equation. The coefficients in this expansion are determined by equations that correspond to the minimization in some sense, of the residual or error in the differential equation. In *boundary collocation*, the role played by the boundary condition and differential equation is reversed. We write

$$\boldsymbol{v}(\boldsymbol{x}) = \sum_n c_n \boldsymbol{v}_{(n)}(\boldsymbol{x}) \ ,$$

i.e., the trial solution is expanded in a complete set of basis functions $\{\boldsymbol{v}_{(n)}\}_1^\infty$. Each $\boldsymbol{v}_{(n)}$ satisfies the governing differential equation, but not the boundary conditions. In *boundary-multipole collocation*, the multipole expansion is used as the basis. The coefficients c_n are determined from the boundary conditions.

The boundary conditions actually provide us with a continuum of equations, one for each surface point. Satisfying all of these is impractical (or viewed in another way, we would then relabel it as a simple problem with an analytical solution), so the numerical procedure is to first truncate the series to finite sums and then enforce some finite set of equations obtained from the boundary conditions to get a linear system determining the unknown coefficients. If these

equations are found by imposing the boundary conditions exactly at a finite number of discrete surface points only, the method is called *collocation.* If in addition derivatives of the boundary conditions with respect to the continuous variables, *i.e.*, location on the surface, are imposed also on discrete surface points, the method of discretizing the continuum of equations is called *osculation.* In *discrete least squares* the equations are formed in a manner similar to collocation, but this is continued until we have an overdetermined system of equations for the coefficients. This system is solved with the ordinary least squares procedure, originally developed by Gauss. One could also approximate a *continuous least squares* procedure numerically with integration quadratures, or try to minimize the maximum residual (*min-max* procedure). In the *method of weighted residuals* the continuous variables are integrated away from the boundary conditions with some weights to get a set of discrete equations for the unknowns. The reader may compare this to determining the Fourier coefficients of a known function, where the resulting linear system is particularly simple. When the weights of integration are chosen to be the same basis functions that the unknowns are multiplying, the procedure is called the *Galerkin method*; this is the most popular of the actual weighted residual methods. It should be clear from the above that once the series expansion has been chosen and truncated, all that remains is a standard curve-fitting problem: We have to find a combination of parameters so that the resulting series approximates the boundary conditions well in some sense. The combination of series expansion and collocation shall be called the *boundary collocation method* (BCM). In Part IV, the BCM for multiparticle cases will be theoretically justified. It will be shown that the disturbance field of a multiparticle system can be uniquely decomposed into disturbance fields of the individual particles, so that single particle basis functions can be used and the system is (analytically) determinate. In practice there are good and bad choices of collocation points, and only rules of thumb, based on generic concepts from interpolation theory, can be given about these.

The application of boundary-multipole collocation to Stokes flow was popularized by the 1971 work of Gluckman *et al.* [21], in which the method was used to solve axisymmetric streaming flow past a collection of spheres and spheroids. One can find earlier applications of the method, *e.g.*, O'Brien's (1968) work on the motion of a slightly deformed drop [58]. Over the subsequent decades, the method has been used to solve a wide range of problems in Stokes flow (a few illustrative examples include: multiple spheres in a cylinder [49]; three-sphere sedimentation problems [18]; two spheroids in a uniform stream [50]; sphere between two plane walls [19, 20]; a sphere in a circular orifice [10]; resistance and mobility functions for two spheres [45]; spheroids and other nonspherical particles settling in a channel [31]; and mobility functions for two spheroids in a linear field [71]). A fairly complete overview of the range of problems that has been successfully tackled by this method during the period 1978–1990 is available in the review article by Weinbaum *et al.* [65].

In general, the boundary-multipole collocation method is a very efficient tool

for the class of Stokes flow involving interactions between particles of simple shape (spheres, spheroids, *etc.*) We illustrate the power of the technique by outlining the steps used to obtain the entire collection of resistance and mobility functions for two spheres of Chapter 11. The results compare favorably with those obtained from other methods, such as separation of variables in bispherical coordinates, method of reflections, and lubrication theory. We also study the convergence of the method, by looking at the boundary collocation solution for a Stokeslet near a sphere.

Perhaps even more impressive is the success of the boundary collocation method for nonaxisymmetric geometries, such as the one formed by two oblate spheroids at arbitrary configurations. The resistance and mobility functions for the two-spheroid problem can be obtained quite readily, even for nearly touching and touching configurations, at a fraction of the computational time required by other methods. Here again, we may gauge the discretization error by comparison with exact analytic solutions for a Stokeslet near a spheroid.

13.2 Two-Sphere Problems

From Chapter 3 we know that the velocity field in any two-sphere Stokes flow problem can be written as a twin multipole expansion about each sphere center. Thus, we are lead to a natural choice for the basis functions for the boundary collocation method: the Stokes multipoles themselves. Since these multipole fields and Lamb's general solution span the same set, we choose, mainly for the sake of ease of notation, to use the latter.

By appropriate choice of $A_{\ell m}$ in the following expression, we obtain all surface velocities associated with disturbance fields of the resistance problem:

$$\boldsymbol{v}_s = \sum_{\ell=1}^{2} \sum_{m=0}^{\ell} \nabla \left[(A_{\ell 0}\delta_{0m} + A_{\ell m} \sin m\phi) r_1^{\ell} P_{\ell}^{m}(\xi_1) \right] . \tag{13.1}$$

Explicitly, if we set all but the following coefficient equal to zero:

1. $A_{10} = 1$ gives a translational velocity along the sphere-sphere axis.

2. $A_{11} = 1$ gives a translational velocity perpendicular to the sphere-sphere axis.

3. $A_{20} = 1$ gives the axisymmetric rate-of-strain field about the sphere-sphere axis.

4. $A_{21} = 1$ gives the hyperbolic straining field associated with the shear flow in the xz-coordinate plane.

5. $A_{22} = 1$ gives the hyperbolic straining field associated with the shear flow in the xy-coordinate plane.

6. $B_{10} = 1$ gives the rotational velocity about the sphere-sphere axis.

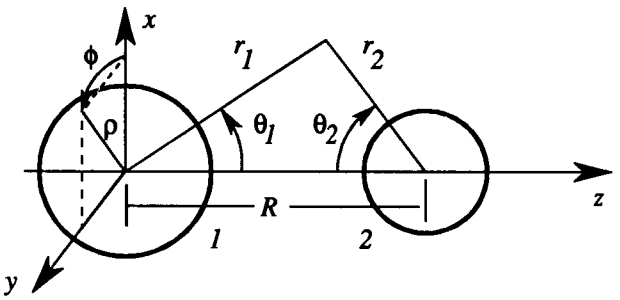

Figure 13.1: The two-sphere geometry.

7. $B_{11} = 1$ gives the rotational velocity about an axis perpendicular to the sphere-sphere axis.

The velocity field must also contain the same ϕ-dependence, so we write Lamb's solution as

$$\begin{aligned} \boldsymbol{v} - \boldsymbol{v}^{\infty} &= \sum_{n=1}^{\infty} \left\{ \frac{n+1}{n(2n-1)} \boldsymbol{r}_\alpha p_{-n-1}^{(\alpha)} - \frac{n-2}{2n(2n-1)} r_\alpha^2 \nabla p_{-n-1}^{(\alpha)} \right. \\ &\quad \left. + \nabla \Phi_{-n-1}^{(\alpha)} + \nabla \times [\boldsymbol{r}_1 \chi_{-n-1}^{(\alpha)}] \right\} , \end{aligned} \tag{13.2}$$

with $\boldsymbol{r}_\alpha = \boldsymbol{x} - \boldsymbol{x}_\alpha$, $r_\alpha = |\boldsymbol{r}_\alpha|$, for $\alpha = 1, 2$, and

$$\begin{aligned} p_{-n-1}^{(\alpha)} &= \sum_{m=0}^{n} (a_{0n}^{(\alpha)} \delta_{0m} + a_{mn}^{(\alpha)} \sin m\phi) r_\alpha^{-(n+1)} P_n^m(\cos\theta_\alpha) \\ \Phi_{-n-1}^{(\alpha)} &= \sum_{m=0}^{n} (b_{0n}^{(\alpha)} \delta_{0m} + b_{mn}^{(\alpha)} \sin m\phi) r_\alpha^{-(n+1)} P_n^m(\cos\theta_\alpha) \\ \chi_{-n-1}^{(\alpha)} &= \sum_{m=0}^{n} c_{mn}^{(\alpha)} r_\alpha^{-(n+1)} P_n^m(\cos\theta_\alpha) \cos m\phi \, . \end{aligned}$$

The two-sphere geometry and the spherical polar angles θ_α and ϕ are shown in Figure 13.1.

Further manipulation of the boundary conditions are required, and these are done more easily in cylindrical coordinates (z, ρ, ϕ) (see Figure 13.1). We may collect terms in $\sin m\phi$ and $\cos m\phi$, and obtain an independent set of equations for each Fourier mode. Thus the ϕ-dependence is eliminated from the problem! The three velocity components yield three independent conditions:

$$\begin{aligned} &\sum_{\alpha=1}^{2} (-1)^\alpha \sum_{n=\ell}^{\infty} \left\{ M_{mn}^{11(\alpha)} a_{mn}^{(\alpha)} + M_{mn}^{12(\alpha)} b_{mn}^{(\alpha)} + M_{mn}^{13(\alpha)} c_{mn}^{(\alpha)} \right\} \\ &\quad = A_{\ell m} \left(\ell \xi_1 P_\ell^m(\xi_1) + (1 - \xi_1^2) P_\ell^{m\prime}(\xi_1) \right) + B_{\ell m} m P_\ell^m(\xi_1) \\ &\sum_{\alpha=1}^{2} (-1)^\alpha \sum_{n=\ell}^{\infty} \left\{ M_{mn}^{21(\alpha)} a_{mn}^{(\alpha)} + M_{mn}^{22(\alpha)} b_{mn}^{(\alpha)} + M_{mn}^{23(\alpha)} c_{mn}^{(\alpha)} \right\} \end{aligned} \tag{13.3}$$

$$= A_{\ell m}\left(\ell \sin\theta_1 P_\ell^m(\xi_1) - [\xi_1 P_\ell^{m+1}(\xi_1) + m \sin\theta_1 P_\ell^m(\xi_1)]\right) - B_{\ell m} P_\ell^{m+1}(\xi_1) \tag{13.4}$$

$$\sum_{\alpha=1}^{2}(-1)^\alpha \sum_{n=\ell}^{\infty}\left\{M_{mn}^{31(\alpha)} a_{mn}^{(\alpha)} + M_{mn}^{32(\alpha)} b_{mn}^{(\alpha)} + M_{mn}^{33(\alpha)} c_{mn}^{(\alpha)}\right\}$$
$$= A_{\ell m} m P_\ell^m(\xi_1)/\sin\theta_1 + B_{\ell m}\sin\theta_1 P_\ell^{m\prime}(\xi_1)\ , \tag{13.5}$$

where

$$\begin{aligned}
M_{mn}^{11(\alpha)} &= r_\alpha^{-n}\left[\frac{n+1}{4n-2}\xi_\alpha P_n^m(\xi_\alpha) - \frac{n-2}{n(4n-2)}(1-\xi_\alpha^2)P_n^{m\prime}(\xi_\alpha)\right]\\
M_{mn}^{12(\alpha)} &= r_\alpha^{-n-2}\left[-(n+1)\xi_\alpha P_n^m(\xi_\alpha) + (1-\xi_\alpha^2)P_n^{m\prime}(\xi_\alpha)\right]\\
M_{mn}^{13(\alpha)} &= r_\alpha^{-n-1} m P_n^m(\xi_\alpha)\\
M_{mn}^{21(\alpha)} &= r_\alpha^{-n}\left[\frac{n+1}{4n-2}\sin\theta_\alpha P_n^m(\xi_\alpha)\right.\\
&\qquad \left. + \frac{n-2}{n(4n-2)}[\xi_\alpha P_n^{m+1}(\xi_\alpha) + m\sin\theta_\alpha P_n^m(\xi_\alpha)]\right]\\
M_{mn}^{22(\alpha)} &= -r_\alpha^{-n-2}\left[(n+1)\sin\theta_\alpha P_n^m(\xi_\alpha)\right.\\
&\qquad \left. + [\xi_\alpha P_n^{m+1}(\xi_\alpha) + m\sin\theta_\alpha P_n^m(\xi_\alpha)]\right]\\
M_{mn}^{23(\alpha)} &= -r_\alpha^{-n-1} P_n^{m+1}(\xi_\alpha)\\
M_{mn}^{31(\alpha)} &= -m r_\alpha^{-n}\frac{n-2}{n(4n-2)}\frac{P_n^m(\xi_\alpha)}{\sin\theta_\alpha}\\
M_{mn}^{32(\alpha)} &= m r_\alpha^{-n-2}\frac{P_n^m(\xi_\alpha)}{\sin\theta_\alpha}\\
M_{mn}^{33(\alpha)} &= r_\alpha^{-n-1}\sin\theta_\alpha P_n^{m\prime}(\xi_\alpha)\ ,
\end{aligned}$$

with $\xi = \cos\theta$ throughout. There is, of course, an analogous set of equations from the boundary conditions on sphere 2.

Equations 13.3 and 13.5 follow directly from the boundary conditions on the z-component and the ϕ-component of the velocity. However, Equation 13.4 is obtained by subtracting the ϕ-component equation from the ρ-component equation. By this maneuver, we ensure that in each equation each term contains the same factor of $\sin\theta_\alpha$, namely, $\sin\theta_\alpha^m$, $\sin\theta_\alpha^{m+1}$, and $\sin\theta_\alpha^{m-1}$, in Equations 13.3–13.5. The importance of this procedure follows from the fact that at $\theta_1 = 0$ and $\theta_1 = \pi$, these factors of $\sin\theta_\alpha$ cause degeneracy ($0 = 0$) in the collocation equations, a problem that is circumvented by first removing these factors of $\sin\theta_\alpha^m$. The benefits gained by placing points at 0 and π are discussed below. Note that on the surface $r_1 = 1$, we have

$$\frac{\sin\theta_2}{\sin\theta_1} = \left[(R+\cos\theta_1)^2 + \sin^2\theta_1\right]^{-1/2}\ ,$$

so that this ratio remains between $R-1$ and $R+1$ for $0 \le \theta_1 \le \pi$.

Now if the multipole expansion is truncated after a finite number of terms, say N_1 and N_2 in the two series, then clearly Equations 13.3–13.5 cannot be

satisfied exactly. The *collocation equations* are obtained by requiring these equalities at N_1 collocation points on sphere 1, *i.e.*, $r_1 = 1$, θ_{1j}, $j = 1, 2, \ldots, N_1$. We do the analogous steps for sphere 2, but with N_2 collocation points. The end result is that with $N_1 + N_2$ collocation points, we obtain $3N_1 + 3N_2$ equations. We also have this many unknowns in the truncated multipole expansions. We note degenerate cases: For axisymmetric streaming flows, the ϕ-component vanishes everywhere and we obtain a degenerate system of order $2N_1 + 2N_2$ by $2N_1 + 2N_2$; for axisymmetric swirling flows, the ϕ-component is the only nonvanishing component so we obtain a degenerate system of order $N_1 + N_2$ by $N_1 + N_2$.

13.2.1 Equal Spheres

For two equal spheres, we reduce the system of equations by exploiting the symmetry with respect to the xy-coordinate plane. An examination of each resistance problem reveals that it possesses one of the following two types of symmetry or may be decomposed into two subproblems, with a subproblem of each symmetry type. A velocity with *mirror symmetry* with respect to the xy-coordinate plane satisfies

$$\begin{aligned} v_x(x,y,z) &= v_x(x,y,-z) \\ v_y(x,y,z) &= v_y(x,y,-z) \\ v_z(x,y,z) &= -v_z(x,y,-z), \end{aligned}$$

i.e., the flow vectors in $z < 0$ and $z > 0$ are mirror images of each other. A field with *mirror anti-symmetry* satisfies

$$\begin{aligned} v_x(x,y,z) &= -v_x(x,y,-z) \\ v_y(x,y,z) &= -v_y(x,y,-z) \\ v_z(x,y,z) &= v_z(x,y,-z). \end{aligned}$$

For such fields, the flow vectors in one half-space is the negative of the mirror image of the vectors in the other half-space.

For problems with these symmetries, the coefficients for the expansion centered at $\boldsymbol{x}_2$ are related to those centered at $\boldsymbol{x}_1$ by the relations,

$$a^{(2)}_{mn} = \mathcal{S} a^{(1)}_{mn} , \qquad b^{(2)}_{mn} = \mathcal{S} b^{(1)}_{mn} , \qquad c^{(2)}_{mn} = \mathcal{S} c^{(1)}_{mn} ,$$

where the symmetry parameter $\mathcal{S}$ is defined by

$$\mathcal{S} = \begin{cases} 1 & \text{for problems with mirror symmetry} \\ -1 & \text{for problems with mirror anti-symmetry.} \end{cases}$$

The collocation solution for these coefficients also satisfy the symmetry condition exactly, *if the collocation points on sphere 2 are placed at the mirror images*

of the points on sphere 1 and the system of equations reduce to two identical subsystems, namely,

$$\begin{aligned}
&\sum_{n=\ell}^{\infty}\Big\{(M_{mn}^{11(1)}-\mathcal{S}M_{mn}^{11(2)})a_{mn}^{(\alpha)}+(M_{mn}^{12(1)}-\mathcal{S}M_{mn}^{12(2)})b_{mn}^{(\alpha)}\\
&\qquad\qquad +(M_{mn}^{13(1)}-\mathcal{S}M_{mn}^{13(2)})c_{mn}^{(\alpha)}\Big\}\\
&\quad = A_{\ell m}\left(\ell\xi_1 P_\ell^m(\xi_1)+(1-\xi_1^2)P_\ell^{m\prime}(\xi_1)\right)+B_{\ell m}mP_\ell^m(\xi_1) \qquad (13.6)\\
&\sum_{\alpha=1}^{2}(-1)^\alpha\sum_{n=\ell}^{\infty}\Big\{(M_{mn}^{21(1)}+\mathcal{S}M_{mn}^{21(2)})a_{mn}^{(\alpha)}+(M_{mn}^{22(1)}+\mathcal{S}M_{mn}^{22(2)})b_{mn}^{(\alpha)}\\
&\qquad\qquad +(M_{mn}^{23(1)}+\mathcal{S}M_{mn}^{23(2)})c_{mn}^{(\alpha)}\Big\}\\
&\quad = A_{\ell m}\left(\ell\sin\theta_1 P_\ell^m(\xi_1)-[\xi_1 P_\ell^{m+1}(\xi_1)+m\sin\theta_1 P_\ell^m(\xi_1)]\right)\\
&\qquad -B_{\ell m}P_\ell^{m+1}(\xi_1) \qquad (13.7)\\
&\sum_{\alpha=1}^{2}(-1)^\alpha\sum_{n=\ell}^{\infty}\Big\{(M_{mn}^{31(1)}+\mathcal{S}M_{mn}^{31(2)})a_{mn}^{(\alpha)}+(M_{mn}^{32(1)}+\mathcal{S}M_{mn}^{32(2)})b_{mn}^{(\alpha)}\\
&\qquad\qquad +(M_{mn}^{33(1)}+\mathcal{S}M_{mn}^{33(2)})c_{mn}^{(\alpha)}\Big\}\\
&\quad = A_{\ell m}mP_\ell^m(\xi_1)/\sin\theta_1+B_{\ell m}\sin\theta_1 P_\ell^{m\prime}(\xi_1)\,. \qquad (13.8)
\end{aligned}$$

13.2.2 Resistance Functions

Given the boundary collocation solution, we now extract the resistance functions, as defined in Chapter 11. Using the relations given in Chapter 4 between the force, torque, and stresslet and the coefficients in Lamb's general solution, we obtain the following expressions for the resistance functions:

$$\begin{aligned}
\widehat{X}_{11}^A &= \frac{1}{3}[a_{01}(1,-1)+a_{01}(1,1)]\\
\widehat{X}_{12}^A &= \frac{1}{3}[a_{01}(1,-1)-a_{01}(1,1)]\\
\widehat{Y}_{11}^A &= \frac{1}{3}[a_{11}(1,-1)+a_{11}(1,1)]\\
\widehat{Y}_{12}^A &= -\frac{1}{3}[a_{11}(1,-1)-a_{11}(1,1)]\\
\widehat{Y}_{11}^B &= -[c_{11}(1,-1)+c_{11}(1,1)]\\
\widehat{Y}_{12}^B &= c_{11}(1,-1)-c_{11}(1,1)\\
\widehat{X}_{11}^G &= -\frac{1}{4}[a_{02}(1,-1)+a_{02}(1,1)]\\
\widehat{X}_{12}^G &= -\frac{1}{4}[a_{02}(1,-1)-a_{02}(1,1)]\\
\widehat{Y}_{11}^G &= -\frac{1}{4}[a_{12}(1,-1)+a_{12}(1,1)]\\
\widehat{Y}_{12}^G &= \frac{1}{4}[a_{12}(1,-1)-a_{12}(1,1)]
\end{aligned}$$

$$\begin{aligned}
\widehat{X}_{11}^{M} + \widehat{X}_{12}^{M} &= \frac{1}{10} a_{02}(2,1) \\
\widehat{Y}_{11}^{M} + \widehat{Y}_{12}^{M} &= \frac{1}{10} a_{12}(2,-1) \\
\widehat{Z}_{11}^{M} + \widehat{Z}_{12}^{M} &= \frac{1}{10} a_{22}(2,1) \; .
\end{aligned}$$

In $a_{mn}(\ell, \mathcal{S})$ and $c_{mn}(\ell, \mathcal{S})$, the index m and argument ℓ denote which $A_{\ell m}$ is set to unity and $\mathcal{S}$ denotes the type of symmetry (or equivalently, a condition placed on the motion of sphere 2).

The remaining resistance functions are associated with rotational motions, and these may be expressed as

$$\begin{aligned}
\widehat{X}_{11}^{C} &= \frac{1}{2}[c_{01}(1,-1) + c_{01}(1,1)] \\
\widehat{X}_{12}^{C} &= -\frac{1}{2}[c_{01}(1,-1) - c_{01}(1,1)] \\
\widehat{Y}_{11}^{C} &= \frac{1}{2}[c_{11}(1,-1) + c_{11}(1,1)] \\
\widehat{Y}_{12}^{C} &= \frac{1}{2}[c_{11}(1,-1) - c_{11}(1,1)] \\
\widehat{Y}_{11}^{H} &= -\frac{1}{8}[a_{12}(1,-1) + a_{12}(1,1)] \\
\widehat{Y}_{12}^{H} &= -\frac{1}{8}[a_{12}(1,-1) - a_{12}(1,1)] \; .
\end{aligned}$$

The index m and argument ℓ now denote which $B_{\ell m}$ is set to unity. The convergence of the method *vs.* the number of collocation points is described in Section 13.3.

13.2.3 Collocation Schemes

We now address the issue of "optimal location" of the collocation points. Although an *a priori* "best" collocation criterion does not exist, for two-sphere problems superior results can be obtained by placing an even number of collocation points uniformly over the meridional chord, as shown in Figure 13.2. We can rationalize this result as follows. The boundary conditions are satisfied only at the collocation points, and nonuniform distributions lead to large, oscillatory deviations from the required boundary conditions in the sparsely collocated region reminiscent of the behavior found in interpolation theory [11]. The implications for the drag calculations, as well the calculations for the higher moments of the tractions, can be seen by using the Lorentz reciprocal theorem in the following manner. We express the error in any multipole moment as an integral of the error in the boundary velocity, weighted by the stress field of the conjugate velocity problem. For example, the error in the force may be written

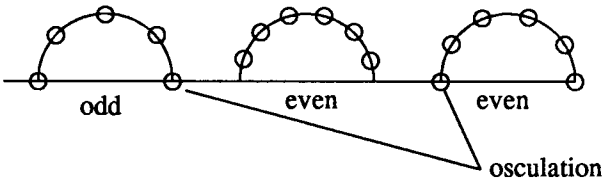

Figure 13.2: Collocation schemes for the two-sphere problem.

as

$$\boldsymbol{F}^{app} - \boldsymbol{F}^{exact} = \oint_S \boldsymbol{v}_{error} \cdot (\boldsymbol{\sigma}(;\boldsymbol{\delta}) \cdot \hat{\boldsymbol{n}})\, dS$$

where $\boldsymbol{\sigma}(;\boldsymbol{\delta}) \cdot \hat{\boldsymbol{n}}$ is the surface traction induced by the constant dyadic "velocity" $\boldsymbol{\delta}$. From this line of reasoning, we conclude that large asymmetric fluctuations in the error velocity field lead to large errors in the multipole moments.

Uniform spacing with an *odd* number of collocation points yield poorer results than that obtained with comparable even numbers. This can be traced to the deterioration in the condition number in the linear system of equations. The point $\theta_1 = \pi/2$ is used when N is odd. Since $P_{2k+1}(\cos\theta_1) = 0$, for all integer k, this collocation point (and equation) places no constraints on the odd coefficients, and in some sense the system is underdetermined. In conclusion, superior results are obtained by uniform placement of an even number of collocation points.

13.3 Error Analysis for Spheres

Since the velocity field in the multisphere problem is generated by a set of multipoles expanded about each sphere center, the essential aspect of the solution is captured by the model problem consisting of a single sphere with a nearby Stokeslet. This "model problem" has an analytical solution, *viz.*, the image system for the Stokeslet near a sphere (see Chapter 10), and thus there are closed-form expressions for all multipole moments. We may compare this with the boundary collocation solution and determine the errors in the numerical method as a function of the adjustable parameters in the numerical scheme. We shall see from these comparisons that the boundary collocation method is quite robust and that the lower order moments, such as the force, torque, and stresslet, are determined quite accurately, even when the Stokeslet is near the sphere.

Throughout this section, we work with the velocity field $\boldsymbol{F} \cdot \mathcal{G}(\boldsymbol{x} - \boldsymbol{x}_2)$ associated with a Stokeslet at $\boldsymbol{x}_2$ *sans* the factor of $8\pi\mu$. We place a stationary,

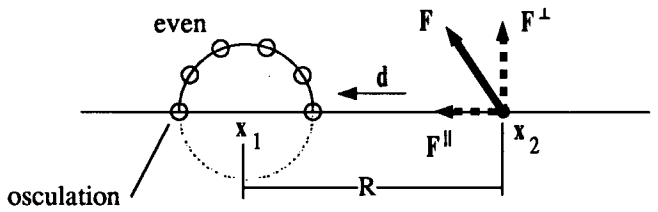

Figure 13.3: Collocation points on a sphere with a Stokeslet nearby.

nonrotating sphere of unit radius centered at $\boldsymbol{x}_1$ and let $R = |\boldsymbol{x}_2 - \boldsymbol{x}_1|$ and $\boldsymbol{d} = (\boldsymbol{x}_1 - \boldsymbol{x}_2)/R$ (see Figure 13.3). We will first consider the axisymmetric case, $\boldsymbol{F}^{\parallel} = \boldsymbol{F} \cdot \boldsymbol{dd}$, and then consider the asymmetric (or transverse) case, $\boldsymbol{F}^{\perp} = \boldsymbol{F} - \boldsymbol{F} \cdot \boldsymbol{dd}$.

13.3.1 Axisymmetric Stokeslet

From Section 10.2, we know that the image system, $\boldsymbol{v}^*$, can be expressed as a multipole expansion,

$$\boldsymbol{v}^* = F d_j \sum_{n=0}^{\infty} \left\{ A_n^{\parallel} \frac{(\boldsymbol{d} \cdot \nabla)^n}{n!} \mathcal{G}_{ij}(\boldsymbol{x} - \boldsymbol{x}_1) + B_n^{\parallel} \frac{(\boldsymbol{d} \cdot \nabla)^n}{n!} \nabla^2 \mathcal{G}_{ij}(\boldsymbol{x} - \boldsymbol{x}_1) \right\} , \quad (13.9)$$

with the coefficients given by

$$\begin{aligned} A_n^{\parallel} &= -(n + \frac{3}{2}) R^{-(n+1)} + (n + \frac{1}{2}) R^{-(n+3)} \\ B_n^{\parallel} &= -\frac{1}{4}(1 - R^2)^2 R^{-(n+5)} . \end{aligned}$$

From Chapter 4, we also have the relation between the multipole expansion and Lamb's general solution. For the latter, we express $\boldsymbol{v}^*$ as

$$\boldsymbol{v}^* = \sum_{n=1}^{\infty} \left\{ -\frac{n-2}{2n(2n-1)} r^2 \nabla p_{-n-1} + \nabla \Phi_{-n-1} \right\} , \quad (13.10)$$

with $p_{-n-1} = a_{0n} r^{-(n+1)} P_n(\cos\theta)$ and $\Phi_{-n-1} = b_{0n} r^{-(n+1)} P_n(\cos\theta)$, and with the relations

$$a_{0n} = -2n A_{n-1}^{\parallel} \qquad b_{0n} = -\frac{n}{2n+3} A_{n+1}^{\parallel} - 2n B_{n-1}^{\parallel} .$$

Combining these relations together, we arrive at the analytical expression for a_{0n} and b_{0n}:

$$\begin{aligned} a_{0n} &= n(2n+1) R^{-n} - n(2n-1) R^{-(n+2)} \\ b_{0n} &= \frac{n}{2} R^{-n} - \frac{n(2n+1)}{2(2n+3)} R^{-(n+2)} . \end{aligned}$$

The boundary collocation solution for the image of the Stokeslet can be obtained with only minor modifications of the collocation equations from the two-sphere problem. We retain the multipole expansion about sphere 1, but for the surface velocity field on sphere 1, we use the velocity field produced by a Stokeslet at $\boldsymbol{x}_2$. The collocation equations are obtained from

$$\sum_{n=1}^{\infty} \left\{ a_{0n} \left[\frac{n+1}{4n-2} \xi_1 P_n(\xi_1) - \frac{n-2}{n(4n-2)} (1-\xi_1^2) P_n'(\xi_1) \right] \right.$$
$$\left. + b_{0n} \left[-(n+1)\xi_1 P_n(\xi_1) + (1-\xi_1^2) P_n'(\xi_1) \right] \right\} = r_2^{-1}(1+\xi_2^2)$$
$$\sum_{n=1}^{\infty} \left\{ a_{0n} \left[\frac{n+1}{4n-2} \sin\theta_1 P_n(\xi_1) + \frac{n-2}{n(4n-2)} [\xi_1 P_n^1(\xi_1) \right] \right.$$
$$\left. - b_{0n} \left[(n+1)\sin\theta_1 P_n(\xi_1) + \xi_1 P_n^1(\xi_1) \right] \right\} = r_2^{-1} \xi_2 \sin\theta_2 \ .$$

In the accompanying tables, the boundary collocation results for a_{0n} and b_{0n} are compared with the analytical results. We examine the influence of the location of the Stokeslet ($R = 1.1, 2.0, 10.0$) and the accuracy obtained with increasing number of collocation points. As expected, fewer collocation points are required with increasing R. For a given R, the solution accuracy degrades with increasing order of the multipole moment. Thus the quantities of greatest interest, such as the force, torque, and stresslet on the particle, may be portrayed quite faithfully with relatively few basis elements. For example, for $R = 2$ and $N = 12$, the relative error in the force (which is proportional to a_{01}) is less than 0.01%. At $R = 1.1$, the 12-point solution still yields the force coefficient accurate to 2%. Similar conclusions may be drawn for the stresslet, which is proportional to a_{02}.

In the tables for $R = 2$, we also show typical results for N odd. As discussed earlier, the collocation equation for the point at $\theta = \pi/2$ do not impose any conditions on the odd coefficients, and the system of equations become ill-conditioned. Consequently, gross errors are produced for the odd coefficients. The even coefficients, nevertheless, are reproduced accurately.

In Figure 13.4, we examine the convergence of a_{01}, *i.e.*, the drag on the sphere, as a function of N. Note that the asymptotic rate of convergence is in line with that expected from interpolation theory.

n	a_{0n} $(exact)$	$N = 12$	$N = 6$
1	0.2990 0000	0.2990 0000	0.2989 9998
2	0.0994 0000	0.0994 0000	0.0994 0013
3	0.0208 5000	0.0208 5000	0.0208 4892
4	0.0035 7200	0.0035 7200	0.0035 6980
5	0.0005 4550	0.0005 4550	0.0005 5489
6	0.0000 7734	0.0000 7734	0.0000 8136
7	0.0000 1041	0.0000 1041	
8	0.0000 0135	0.0000 0135	
9	0.0000 0017	0.0000 0017	
	⋮	⋮	
12	2.97×10^{-10}	3.06×10^{-10}	

n	b_{0n} $(exact)$	$N = 12$	$N = 6$
1	0.0497 0000	0.0497 0000	0.0497 0004
2	0.0099 2857	0.0099 2857	0.0099 2855
3	0.0014 8833	0.0014 8833	0.0014 8814
4	0.0001 9836	0.0001 9836	0.0001 9829
5	0.0000 2479	0.0000 2479	0.0000 2528
6	0.0000 0297	0.0000 0297	0.0000 0310
7	0.0000 0035	0.0000 0035	
8	0.0000 0004	0.0000 0004	
	⋮	⋮	
12	5.94×10^{-12}	6.11×10^{-12}	

Table 13.1: Axisymmetric Stokeslet at $R = 10$ for 6 and 12 collocation points.

n	a_{0n} (*exact*)	$N = 13$	$N = 12$	$N = 6$
1	1.3750 000	1.50×10^{7}	1.3749 948	1.3728 351
2	2.1250 000	2.1249 949	2.1250 092	2.1265 069
3	2.1562 500	3.28×10^{8}	2.1561 516	2.0732 118
4	1.8125 000	1.8123 653	1.8126 081	1.6942 577
5	1.3671 875	1.61×10^{9}	1.3667 642	2.1913 532
6	0.9609 3750	0.9606 1693	0.9617 2449	1.6017 759
7	0.6425 7813	7.33×10^{9}	0.6409 8340	
8	0.4140 6250	0.4128 0571	0.4240 3929	
9	0.2592 7734	6.45×10^{10}	0.2489 1388	
10	0.1586 9141	0.1582 7188	0.0929 1618	
11	0.0953 3691	-3.50×10^{11}	0.1507 9108	
12	0.0563 9648	0.0825 1236	0.1412 5853	

n	b_{0n} (*exact*)	$N = 13$	$N = 12$	$N = 6$
1	0.2125 0000	-7.49×10^{6}	0.2125 0359	0.2127 2613
2	0.2053 5714	0.2053 6018	0.2053 5866	0.1995 4268
3	0.1510 4167	1.09×10^{7}	0.1510 4105	0.1363 7757
4	0.0994 3182	0.0994 2728	0.0994 3845	0.0980 2443
5	0.0615 9856	5.38×10^{7}	0.0615 8859	0.1047 1251
6	0.0367 1875	0.0367 1154	0.0367 4256	0.0603 6923
7	0.0213 1204	2.01×10^{8}	0.0212 6457	
8	0.0121 2993	0.0120 9749	0.0123 1510	
9	0.0068 0106	1.48×10^{9}	0.0064 1732	
10	0.0037 6826	0.0036 8745	0.0024 1398	
11	0.0020 6787	-6.81×10^{9}	0.0033 5303	
12	0.0011 2576	0.0016 9952	0.0027 2114	

Table 13.2: Axisymmetric Stokeslet at $R = 2$ for 6, 12, and 13 collocation points.

n	a_{0n} (*exact*)	$N = 48$	$N = 12$
1	1.9759 579	1.9758 626	1.9978 184
2	4.1663 821	4.1663 929	3.9983 077
3	6.4637 910	6.4621 287	6.6397 658
4	8.7832 144	8.7833 387	6.7645 759
5	11.0585 57	11.0533 37	10.6850 73
	⋮	⋮	⋮
12	22.9098 19	22.9173 03	-3.00×10^2
	⋮	⋮	
48	9.1468 796	1.02×10^3	

n	b_{0n} (*exact*)	$N = 48$	$N = 12$
1	0.2291 5101	0.2291 9937	0.2047 3955
2	0.3385 7952	0.3385 8059	0.3138 8465
3	0.4025 6398	0.4025 1006	0.3729 7097
4	0.4423 4230	0.4423 4850	0.3161 6323
5	0.4667 7651	0.4666 0456	0.3827 8957
	⋮	⋮	⋮
12	0.4488 3352	0.4489 6889	−4.8118 295
	⋮	⋮	
48	0.0470 6371	5.1354 072	

Table 13.3: Axisymmetric Stokeslet at $R = 1.1$ for 12 and 48 collocation points.

13.3.2 The Transverse Stokeslet

We now consider the transverse case $\boldsymbol{F} = \boldsymbol{F}^{\perp}$ with $\boldsymbol{F}^{\perp} \cdot \boldsymbol{d} = 0$. With $\boldsymbol{t} = \boldsymbol{F}^{\perp} \times \boldsymbol{d}$, we have the two velocity representations:

$$\begin{aligned} v_i^* &= F_j \sum_{n=0}^{\infty} \left\{ A_n^{\perp} \frac{(\boldsymbol{d} \cdot \nabla)^n}{n!} \mathcal{G}_{ij}(\boldsymbol{x} - \boldsymbol{x}_1) + B_n^{\perp} \frac{(\boldsymbol{d} \cdot \nabla)^n}{n!} \nabla^2 \mathcal{G}_{ij}(\boldsymbol{x} - \boldsymbol{x}_1) \right\} \\ &\quad + \epsilon_{ijk} t_j \sum_{n=0}^{\infty} C_n^{\perp} \frac{(\boldsymbol{d} \cdot \nabla)^n}{n!} \frac{\partial}{\partial x_k} \frac{1}{r_1} \end{aligned} \tag{13.11}$$

and

$$\begin{aligned} \boldsymbol{v}^* &= \sum_{n=1}^{\infty} \left\{ -\frac{n-2}{2n(2n-1)} r^2 \nabla p_{-n-1} + \nabla \Phi_{-n-1} \right. \\ &\quad \left. + \nabla \times [(\boldsymbol{x} - \boldsymbol{x}_1) \chi_{-n-1}] \right\} , \end{aligned} \tag{13.12}$$

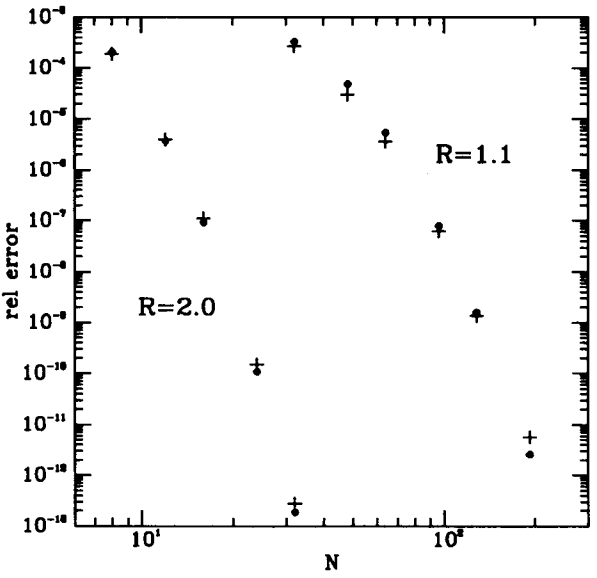

Figure 13.4: Convergence of a_{01} (•) and a_{11} (+) *vs.* number of points.

with

$$\begin{aligned} p_{-n-1} &= a_{1n} r^{-(n+1)} P_n^1(\cos\theta) \sin\phi \\ \Phi_{-n-1} &= b_{1n} r^{-(n+1)} P_n^1(\cos\theta) \sin\phi \\ \chi_{-n-1} &= c_{1n} r^{-(n+1)} P_n^1(\cos\theta) \cos\phi \ . \end{aligned}$$

From Section 10.2, the multipole expansion coefficients are:

$$A_n^{\perp} = \frac{(n-1)(2n+3)}{2(n+2)} R^{-(n+1)} - \frac{(n+1)(2n+1)}{2(n+2)} R^{-(n+3)} \tag{13.13}$$

$$B_n^{\perp} = \frac{(n-1)}{4(n+2)} R^{-(n+1)} - \left[\frac{(n-1)}{4(n+2)} + \frac{(n+1)}{4(n+4)}\right] R^{-(n+3)} \tag{13.14}$$

$$C_n^{\perp} = \frac{2n+3}{n+3} R^{-(n+2)} - \frac{2n+3}{n+3} R^{-(n+4)} \ . \tag{13.15}$$

These coefficients are related to those in Lamb's solution by the following:

$$a_{1n} = 2A_{n-1}^{\perp} \tag{13.16}$$

$$c_{1n} = \frac{1}{n} C_{n-1}^{\perp} - \frac{2}{n(n+1)} A_n^{\perp} \tag{13.17}$$

$$b_{1n} = 2B_{n-1}^{\perp} - \frac{1}{n+1} C_n^{\perp} + \frac{(n+3)}{(n+1)(2n+3)} A_{n+1}^{\perp} \ , \tag{13.18}$$

so that

$$a_{1n} = \frac{(n-2)(2n+1)}{(n+1)} R^{-n} - \frac{n(2n-1)}{(n+1)} R^{-(n+2)} \tag{13.19}$$

$$b_{1n} = \frac{(n-2)}{2(n+1)} R^{-n} - \frac{n(2n+1)}{2(n+1)(2n+3)} R^{-(n+2)} \tag{13.20}$$

$$c_{1n} = \frac{2}{n(n+1)} R^{-(n+1)} \, . \tag{13.21}$$

For the transverse Stokeslet, the collocation equations are

$$\begin{aligned}
&\sum_{n=1}^{\infty} \left\{ a_{1n} \left[\frac{n+1}{4n-2} \xi_1 P_n^1(\xi_1) - \frac{n-2}{n(4n-2)} (1-\xi_1^2) P_n^{1\prime}(\xi_1) \right] \right. \\
&\qquad \left. + b_{1n} \left[-(n+1)\xi_1 P_n^1(\xi_1) + (1-\xi_1^2) P_n^{1\prime}(\xi_1) \right] + c_{1n} P_n^1(\xi_1) \right\} \\
&\quad = r_2^{-1} \xi_2 \sin\theta_2 \\
&\sum_{n=1}^{\infty} \left\{ a_{1n} \left[\frac{n+1}{4n-2} \sin\theta_1 P_n(\xi_1) + \frac{n-2}{n(4n-2)} [\xi_1 P_n^2(\xi_1) + \sin\theta_1 P_n^1(\xi_1)] \right] \right. \\
&\qquad \left. - b_{1n} \left[(n+2) \sin\theta_1 P_n^1(\xi_1) + \xi_1 P_n^2(\xi_1) \right] - c_{1n} P_n^2(\xi_1) \right\} \\
&\quad = r_2^{-1} \sin^2\theta_2 \\
&\sum_{n=1}^{\infty} \left\{ -a_{1n} \frac{n-2}{n(4n-2)} \frac{P_n^1(\xi_1)}{\sin\theta_1} \right. \\
&\qquad \left. + b_{1n} \frac{P_n^1(\xi_1)}{\sin\theta_1} + c_{1n} \sin\theta_1 P_n^{1\prime}(\xi_1) \right\} = r_2^{-1} \, .
\end{aligned}$$

In the accompanying tables, these exact results for the coefficients are compared with the corresponding boundary collocation results. Again, we conclude that the numerical results remain accurate even when the Stokeslet is quite near the sphere and that the lower order moments, such as the force, torque, and stresslet, are obtained with higher accuracy than the overall solution.

In Figure 13.4, we examine the convergence of a_{11}, which is proportional to the drag on the sphere, as a function of N, and, as in the axisymmetric problem, the rate of convergence is reminiscent of that found in interpolation theory.

n	a_{1n} (*exact*)	$N = 12$	$N = 6$
1	−0.1505 0000	−0.1505 0000	−0.1505 0001
2	−0.0002 0000	−0.0002 0000	−0.0001 9999
3	0.0017 1250	0.0017 1250	0.0017 1227
4	0.0003 5440	0.0003 5440	0.0003 5425
5	0.0000 5425	0.0000 5425	0.0000 5542
6	0.0000 0733	0.0000 0733	0.0000 0759
	⋮	⋮	
12	1.90×10^{-11}	1.96×10^{-11}	

n	b_{1n} (*exact*)	$N = 12$	$N = 6$
1	−0.0251 5000	−0.0251 5000	−0.0251 5001
2	−0.0000 2381	−0.0000 2381	−0.0000 2380
3	0.0001 2208	0.0001 2208	0.0001 2208
4	0.0000 1967	0.0000 1967	0.0000 1966
5	0.0000 0246	0.0000 0246	0.0000 0251
6	0.0000 0028	0.0000 0028	0.0000 0029
	⋮	⋮	
12	3.80×10^{-13}	3.92×10^{-13}	

n	c_{1n} (*exact*)	$N = 12$	$N = 6$
1	0.0100 0000	0.0100 0000	0.0100 0000
2	0.0003 3333	0.0003 3333	0.0003 3335
3	0.0000 1667	0.0000 1667	0.0000 1666
4	0.0000 0100	0.0000 0100	0.0000 0097
5	6.67×10^{-8}	6.67×10^{-8}	6.78×10^{-8}
6	4.76×10^{-9}	4.76×10^{-9}	1.69×10^{-8}
	⋮	⋮	
12	1.28×10^{-15}	8.46×10^{-15}	

Table 13.4: Transverse Stokeslet at $R = 10$ for 6 and 12 collocation points.

n	a_{1n} $(exact)$	$N = 12$	$N = 6$
1	−0.8125 0000	−0.8125 0321	−0.8138 0688
2	−0.1250 0000	−0.1249 9819	−0.1194 9522
3	0.1015 6250	0.1015 4305	0.0709 9711
4	0.1375 0000	0.1375 1330	0.0528 2180
5	0.1132 8125	0.1132 3093	0.2268 4604
6	0.0792 4107	0.0793 0014	0.2113 7383
	⋮	⋮	
12	0.0033 9919	0.0077 6035	

n	b_{1n} $(exact)$	$N = 12$	$N = 6$
1	−0.1437 5000	−0.1437 5201	−0.1440 5275
2	−0.0148 8095	−0.0148 8105	−0.0126 8696
3	0.0065 1042	0.0065 0795	0.0053 0967
4	0.0073 8636	0.0073 8688	0.0009 5563
5	0.0050 5809	0.0050 5478	0.0097 0791
6	0.0030 1339	0.0030 1613	0.0086 1188
	⋮	⋮	
12	6.78×10^{-5}	1.59×10^{-4}	

n	c_{1n} $(exact)$	$N = 12$	$N = 6$
1	0.2500 0000	0.2500 0013	0.2492 3892
2	0.0416 6667	0.0416 6886	0.0436 6289
3	0.0104 1667	0.0104 1668	0.0096 3527
4	0.0031 2500	0.0031 2670	−0.0009 2969
5	0.0010 4167	0.0010 4160	0.0016 8348
6	0.0003 7202	0.0003 7438	0.0020 8919
	⋮	⋮	
12	1.56×10^{-6}	1.60×10^{-5}	

Table 13.5: Transverse Stokeslet at $R = 2$ for 6 and 12 collocation points.

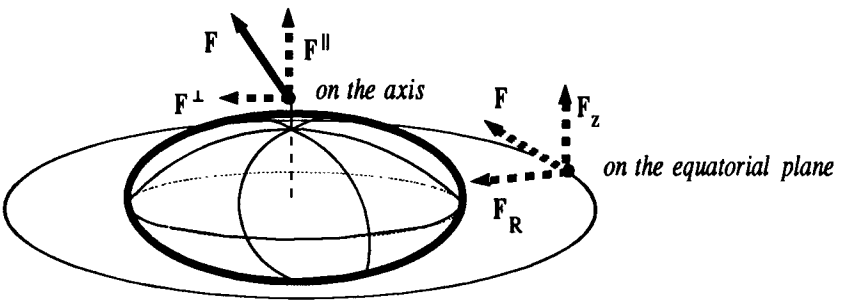

Figure 13.5: The Stokeslet near a stationary oblate spheroid.

13.4 Error Analysis for Spheroids

We examine the problem of a Stokeslet placed near an oblate spheroid to gauge the accuracy of the boundary collocation solution. The principles involved are the same as those discussed previously for the sphere.

From Chapter 3, we have the following expression (Faxén law) for the force on a stationary oblate spheroid in the field produced by the Stokeslet:

$$\begin{aligned} \boldsymbol{F}^S &= 6\pi\mu a[X^A \boldsymbol{dd} + Y^A(\boldsymbol{\delta} - \boldsymbol{dd})] \cdot \left\{ \frac{\sin D_z}{D_z} \right. \\ &\quad \left. - \frac{a^2}{2}\left(\frac{1}{D_z}\frac{\partial}{\partial D_z}\right)\frac{\sin D_z}{D_z}\nabla^2 \right\} \boldsymbol{F} \cdot \frac{\mathcal{G}(\boldsymbol{x} - \boldsymbol{x}_2)}{8\pi\mu}|_{x=x_1} , \end{aligned} \tag{13.22}$$

where $D_z^2 = (a^2 - c^2)\partial^2/\partial z^2$ and the resistance functions X^A and Y^A are as defined in Chapter 5. Where expedient, we will write the radius of the focal disk, $(a^2 - c^2)^{1/2} = ae$ as a_E. We will also use e to denote the eccentricity of the spheroid.

In comparison with the analysis for spheres, the spheroid problem inevitably requires more geometric parameters. Note also that if the Stokeslet is off the symmetry axis of the spheroid, then the spheroid-Stokeslet geometry is not axisymmetric. Thus the complete solution will depend on the numerous parameters that specify the location of the Stokeslet relative to the spheroid. However, our interest here is only in the exposition of the accuracy of the collocation solutions, and this information may be extracted by examining two special configurations: a Stokeslet placed on the axis of symmetry and a Stokeslet placed on the "equatorial plane," as shown in Figure 13.5. The collocation scheme is also depicted in the figure.

n	a_{1n} (*exact*)	$N = 48$	$N = 12$
1	−1.7392 938	−1.7393 460	−1.7960 163
2	−1.3660 269	−1.3659 905	−1.1717 432
3	−1.0136 541	−1.0139 570	−1.4739 896
4	−0.7022 0558	−0.7021 0205	0.0332 0390
5	−0.4336 1861	−0.4341 8951	−1.7801 860
6	−0.2052 6349	−0.2050 7080	2.8300 659
	⋮	⋮	⋮
12	0.5367 9068	0.5374 4096	1.51×10^2
	⋮	⋮	
48	0.1458 6194	0.1440 3522	

n	b_{1n} (*exact*)	$N = 48$	$N = 12$
1	−0.3399 6995	−0.3399 9637	−0.3625 6759
2	−0.1626 2225	−0.1626 1649	−0.1232 1870
3	−0.0871 8770	−0.0872 1832	−0.1256 7090
4	−0.0481 3422	−0.0481 2714	0.0135 7631
5	−0.0256 9080	−0.0257 2281	−0.0904 0912
6	−0.0119 9590	−0.0119 8742	0.1399 9798
	⋮	⋮	⋮
12	0.0100 1559	0.0100 2978	3.2409 243
	⋮	⋮	
48	0.0007 5013	0.0755 4548	

n	c_{1n} (*exact*)	$N = 48$	$N = 12$
1	0.8264 4628	0.8264 3625	0.7679 1789
2	0.2504 3827	0.2504 6764	0.2860 8967
3	0.1138 3558	0.1138 3157	0.0885 8993
4	0.0620 9213	0.0621 0825	0.0965 2831
5	0.0376 3160	0.0376 2896	0.0177 1595
6	0.0244 3610	0.0244 4747	0.0853 5150
	⋮	⋮	⋮
12	0.0037 1365	0.0037 2040	0.5079 2543
	⋮	⋮	
48	7.97×10^{-6}	2.89×10^{-3}	

Table 13.6: Transverse Stokeslet at $R = 1.1$ for 12 and 48 collocation points.

13.4.1 Stokeslet on the Axis

We now show that a Stokeslet of strength $\boldsymbol{F}$ placed on the axis of symmetry exerts a force $\boldsymbol{F}^S$ given by

$$\begin{aligned}\boldsymbol{F}^S &= \boldsymbol{F}\cdot\boldsymbol{dd}\frac{3X^A}{4e^3}\left[(2e^2-1)\cot^{-1}(R/ae)+\frac{eR/a}{(R/a)^2+e^2}\right]\\ &\quad+(\boldsymbol{F}-\boldsymbol{F}\cdot\boldsymbol{dd})\frac{3Y^A}{8e^3}\left[(2e^2+1)\cot^{-1}(R/ae)-\frac{eR/a}{(R/a)^2+e^2}\right]\end{aligned}$$

on the stationary spheroid. Since $R=|\boldsymbol{x}_2-\boldsymbol{x}_1|$ is the separation between the spheroid center and the Stokeslet, we assume $c<R<\infty$. The two lines on the RHS of the preceding equation correspond to Stokeslet orientions along and perpendicular to the symmetry axis.

Stokeslet Aligned with the Axis

If we have $\boldsymbol{F}=\boldsymbol{F}^{\parallel}$, *i.e.*, the Stokeslet is aligned with the symmetry axis, then only the axial component is nonzero. We employ the following expressions for $\partial^n\mathcal{G}/\partial z^n$ from Chapter 3:

$$\begin{aligned}\frac{(\boldsymbol{d}\cdot\nabla)^n}{n!}\boldsymbol{F}^{\parallel}\cdot\mathcal{G}(\boldsymbol{x}-\boldsymbol{x}_2)|_{x=x_1} &= 2\boldsymbol{F}^{\parallel}R^{-(n+1)}\\ \frac{(\boldsymbol{d}\cdot\nabla)^n}{n!}\boldsymbol{F}^{\parallel}\cdot\nabla^2\mathcal{G}(\boldsymbol{x}-\boldsymbol{x}_2)|_{x=x_1} &= -2(n+1)(n+2)\boldsymbol{F}^{\parallel}R^{-(n+3)}\end{aligned}$$

to reduce Equation 13.22 to

$$F^S=F^{\parallel}\frac{3}{2}X^A\frac{a}{R}\sum_{k=0}^{\infty}(-1)^k\left[\frac{1}{2k+1}-\frac{a^2}{R^2}\frac{k+1}{2k+3}\right]\left(\frac{a_E}{R}\right)^{2k}. \qquad (13.23)$$

Note that the infinite series in R^{-1} converges only if $R^{-1}\le a_E$. We may visualize this constraint with the help of a "hemispheric dome" of radius a_E over the focal circle of the spheroid. If we move the Stokeslet along the axis of symmetry, the infinite series will converge only if the Stokeslet lies outside the hemisphere. In general, when the Faxén law is written as an infinite series in differential operators, the resulting expression will have a finite radius of convergence in R^{-1}, and, furthermore, this expression will fail to converge when the Stokeslet is too close to the particle. This example also shows that the exact value of the radius of convergence depends on the details of the particle geometry. *In particular, this value corresponds neither to the particle surface nor the surface of the "effective sphere" that circumscribes the particle.*

In Chapter 3, we showed other forms for the Faxén relation for the ellipsoid that did not require an infinite series expansion in differential operators. The final expression for the force obtained from these alternate forms will be an analytic function of R that converges for all physical values of R. In principle, we may obtain these force expressions starting from the appropriate Faxén

relation. However, it is easier to use analytic continuation of Equation 13.23 to reproduce these results. We replace the infinite series by using the identities

$$\sum_{k=0}^{\infty} \frac{(-1)^k}{2k+1} x^{2k} = x^{-1} \cot^{-1} x^{-1}$$

$$\sum_{k=0}^{\infty} (-1)^k \frac{2k+2}{2k+1} x^{2k} = \frac{1}{1+x^2} - x^{-2} + x^{-3} \cot^{-1} x^{-1}$$

to obtain

$$F^S = F^{\parallel} \frac{3X^A}{4e^3} \left[(2e^2 - 1) \cot^{-1}(R/ae) + \frac{eR/a}{(R/a)^2 + e^2} \right] . \tag{13.24}$$

In the limiting case $R \to c$, this reduces to $F^S \to F^{\parallel}$, and when $e \to 0$ we recover the result for the sphere,

$$F^S = F^{\parallel} \left[\frac{3}{2} \frac{a}{R} - \frac{1}{2} \left(\frac{a}{R} \right)^3 \right] .$$

Stokeslet Perpendicular to the Axis

If $\boldsymbol{F} = \boldsymbol{F}^{\perp}$ with $\boldsymbol{F}^{\perp} \cdot \boldsymbol{d} = 0$, then only the component parallel to $\boldsymbol{F}^{\perp}$ is nonzero, and with the help of

$$\begin{aligned} \frac{(\boldsymbol{d} \cdot \nabla)^n}{n!} \boldsymbol{F}^{\perp} \cdot \mathcal{G}(\boldsymbol{x} - \boldsymbol{x}_2)|_{x=x_1} &= \boldsymbol{F}^{\perp} R^{-(n+1)} \\ \frac{(\boldsymbol{d} \cdot \nabla)^n}{n!} \boldsymbol{F}^{\perp} \cdot \nabla^2 \mathcal{G}(\boldsymbol{x} - \boldsymbol{x}_2)|_{x=x_1} &= (n+1)(n+2) \boldsymbol{F}^{\perp} R^{-(n+3)} , \end{aligned}$$

Equation 13.22 reduces to

$$F^S = F^{\perp} \frac{3}{4} Y^A \frac{a}{R} \sum_{k=0}^{\infty} (-1)^k \left[\frac{1}{2k+1} + \frac{a^2}{R^2} \frac{k+1}{2k+3} \right] \left(\frac{a_E}{R} \right)^{2k} . \tag{13.25}$$

Again, the radius of convergence is at $R^{-1} = a_E$. The expression that is valid for all $R^{-1} \geq c$ is

$$F^S = F^{\perp} \frac{3Y^A}{8e^3} \left[(2e^2 + 1) \cot^{-1}(R/ae) - \frac{eR/a}{(R/a)^2 + e^2} \right] . \tag{13.26}$$

The limiting cases give consistent results. When $R \to c$, we obtain $F^S \to F^{\perp}$, and when $e \to 0$ we recover the result for the sphere,

$$F^S = F^{\perp} \left[\frac{3}{4} \frac{a}{R} + \frac{1}{4} \left(\frac{a}{R} \right)^3 \right] .$$

In Figure 13.6 the exact solutions for the force are compared with those obtained by boundary collocation. We see that even when the solution is expanded only up to (distributed) quadrupoles, the collocation solutions reproduce the net force accurately for all Stokeslets, except those placed very close to the surface.

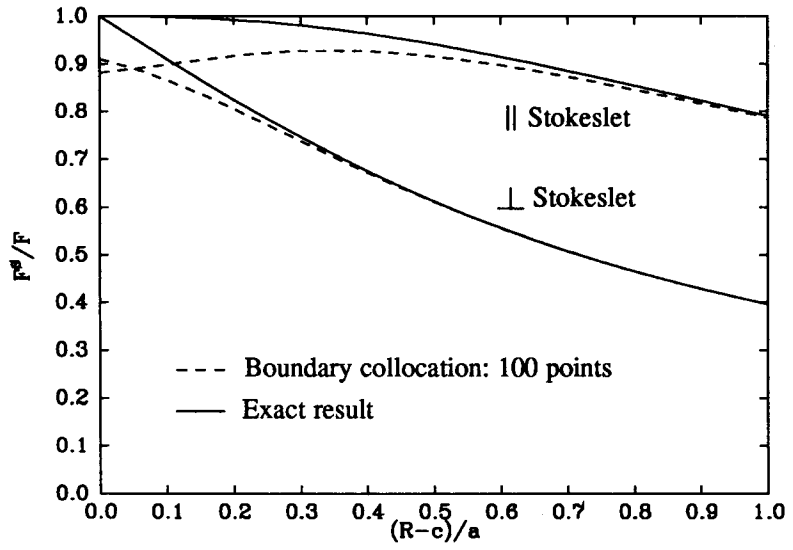

Figure 13.6: Force on an oblate spheroid due to a nearby Stokeslet: comparison of exact and collocation results.

13.4.2 Stokeslet on the Equatorial Plane

If the Stokeslet is in the equatorial plane, it is convenient to decompose the problem into three special cases in which the Stokeslet is aligned with the basis vectors e_z, e_R, and e_ϕ of the cylindrical coordinate system. Keeping in mind that $a < R < \infty$, the final result for the force on the spheroid may be written as

$$\begin{aligned} \boldsymbol{F}^S &= \boldsymbol{F}\cdot\boldsymbol{dd}\frac{3X^A}{4e^3}\left[(2e^2-1)\chi+(1-e^2)\frac{ae}{(R^2-a^2e^2)^{1/2}}\right] \\ &\quad + \boldsymbol{F}\cdot\boldsymbol{e}_R\boldsymbol{e}_R\frac{3Y^A}{8e^3}\left[(2e^2+1)\chi+\frac{(2e^2-1)ae-a^3e^3/R^2}{(R^2-a^2e^2)^{1/2}}\right] \\ &\quad + \boldsymbol{F}\cdot\boldsymbol{e}_\phi\boldsymbol{e}_\phi\frac{3Y^A}{8e^3}\left[(2e^2+1)\chi-e\frac{a}{R}[1-e^2(a/R)^2]^{1/2}\right] , \end{aligned}$$

where

$$\chi = \cot^{-1}\left(\frac{\sqrt{(R/a)^2-e^2}}{e}\right) . \tag{13.27}$$

We now consider the three cases.

Stokeslet Aligned with the Axis

If the Stokeslet is aligned with the symmetry axis, then only the axial component of the force on the spheroid is nonzero. We use

$$\begin{aligned}\frac{(\boldsymbol{d}\cdot\nabla)^n}{n!}F_z\boldsymbol{e}_z\cdot\mathcal{G}(\boldsymbol{x}-\boldsymbol{x}_2)|_{x=x_1} &= -(n-1)F_z\boldsymbol{e}_z\frac{P_n(0)}{R^{n+1}}\\ \frac{(\boldsymbol{d}\cdot\nabla)^n}{n!}F_z\boldsymbol{e}_z\cdot\nabla^2\mathcal{G}(\boldsymbol{x}-\boldsymbol{x}_2)|_{x=x_1} &= -2(n+1)(n+2)F_z\boldsymbol{e}_z\frac{P_{n+2}(0)}{R^{n+3}}\end{aligned}$$

to reduce Equation 13.22 to

$$F^S = F_z\frac{3}{4}X^A\frac{a}{R}\sum_{k=0}^{\infty}(-1)^k\left[P_{2k}(0)\frac{1-2k}{2k+1}-\frac{a^2}{R^2}P_{2k+2}(0)\frac{2k+2}{2k+3}\right]\left(\frac{a_E}{R}\right)^{2k} \tag{13.28}$$

Now, identities such as

$$\sum_{k=0}^{\infty}(-1)^kP_{2k}(0)x^{2k} = (1-x^2)^{-1/2}$$

$$\sum_{k=0}^{\infty}\frac{(-1)^kP_{2k}(0)}{2k+1}x^{2k+1} = \cot^{-1}\left(\frac{(1-x^2)^{1/2}}{x}\right)$$

may be used to replace Equation 13.28 with

$$F^S = F_z\frac{3X^A}{4e^3}\left[(2e^2-1)\chi+(1-e^2)\frac{ae}{(R^2-a^2e^2)^{1/2}}\right], \tag{13.29}$$

with χ as defined previously in Equation 13.27. For $R\to a$, $F^S\to F_z$, and $e\to 0$ we recover the result for the transverse Stokeslet near a sphere.

Stokeslet in the Radial Direction

For $\boldsymbol{F} = F_R\boldsymbol{e}_R$ (see Figure 13.5) only the R-component of the force on the spheroid is nonzero. We use

$$\begin{aligned}\boldsymbol{e}_R\cdot\frac{(\boldsymbol{d}\cdot\nabla)^n}{n!}\boldsymbol{F}\cdot\mathcal{G}(\boldsymbol{x}-\boldsymbol{x}_2)|_{x=x_1} &= (n+2)F_R\frac{P_n(0)}{R^{n+1}}\\ \boldsymbol{e}_R\cdot\frac{(\boldsymbol{d}\cdot\nabla)^n}{n!}\boldsymbol{F}\cdot\nabla^2\mathcal{G}(\boldsymbol{x}-\boldsymbol{x}_2)|_{x=x_1} &= -2(n+1)(n+2)F_R\frac{P_n(0)}{R^{n+3}}\end{aligned}$$

to reduce Equation 13.22 to

$$F^S = F_R\frac{3}{4}Y^A\frac{a}{R}\sum_{k=0}^{\infty}(-1)^kP_{2k}(0)\left[\frac{2k+2}{2k+1}-\frac{a^2}{R^2}\frac{2k+2}{2k+3}\right]\left(\frac{a_E}{R}\right)^{2k}. \tag{13.30}$$

We may rewrite Equation 13.30 as

$$F^S = F_R\frac{3Y^A}{8e^3}\left[(2e^2+1)\chi+\frac{(2e^2-1)ae-a^3e^3/R^2}{(R^2-a^2e^2)^{1/2}}\right], \tag{13.31}$$

with χ as defined previously in Equation 13.27. In the limiting case $R\to a$ this reduces to $F^S\to F_R$, and when $e\to 0$ we recover the result for the axisymmetric Stokeslet near a sphere.

Stokeslet in the Azimuthal Direction

For $\boldsymbol{F} = F_\phi \boldsymbol{e}_\phi$ only the ϕ-component of the force on the spheroid is nonzero. We use

$$\begin{aligned} \boldsymbol{e}_\phi \cdot \frac{(\boldsymbol{d}\cdot\nabla)^n}{n!}\boldsymbol{F}\cdot\mathcal{G}(\boldsymbol{x}-\boldsymbol{x}_2)|_{x=x_1} &= F_\phi R^{-(n+1)}P_n(0) \\ \boldsymbol{e}_\phi \cdot \frac{(\boldsymbol{d}\cdot\nabla)^n}{n!}\boldsymbol{F}\cdot\nabla^2\mathcal{G}(\boldsymbol{x}-\boldsymbol{x}_2)|_{x=x_1} &= 2(n+1)F_\phi R^{-(n+3)}P_n(0) \end{aligned}$$

to reduce Equation 13.22 to

$$F^S = F_\phi \frac{3}{4}Y^A \frac{a}{R}\sum_{k=0}^{\infty}(-1)^k P_{2k}(0)\left[\frac{1}{2k+1}+\frac{a^2}{R^2}\frac{1}{2k+3}\right]\left(\frac{a_E}{R}\right)^{2k}. \qquad (13.32)$$

We may rewrite Equation 13.32 as

$$F^S = F_\phi \frac{3Y^A}{8e^3}\left[(2e^2+1)\chi - e\frac{a}{R}[1-e^2(a/R)^2]^{1/2}\right]. \qquad (13.33)$$

In the limiting case $R \to a$, this reduces to $F^S \to F_\phi$, and when $e \to 0$ we recover the result for the transverse Stokeslet near a sphere.

In Figure 13.6, the exact solutions for the force are compared with those obtained by boundary collocation. Here also, the collocation solutions reproduce the net force accurately for all Stokeslets except those placed very close to the spheroid.

We conclude this chapter on boundary-multipole collocation by stating that the basis functions are the key to the success of the method. In the extreme limit where the exact analytical solution is known (let us denote it as $c_1 \boldsymbol{v}_{(1)}$), then a one-point collocation of the one-term expansion, $\boldsymbol{v} = c_1 \boldsymbol{v}_{(1)}$, would work. More generally, a good basis set gives a rapidly converging expansion so that accurate solutions are obtained with a small number of unknown coefficients. In the case of ellipsoids and spheroids, the use of Lamb's general solution or any other expansion based on the spherical harmonics is a bad idea; from Chapter 3 we know that even the translating ellipsoid has a slowly converging infinite series expansion of this type. On the other hand, it should be apparent from the discussion in this section that expansions based on the singularity solutions of Chapter 3 should work quite nicely. The recent work by Yoon and Kim [71] demonstrate that this is indeed the case.

Exercises

Exercise 13.1 Stokeslet Near a Spheroid.
Show that the results in Section 13.4 for the force on a spheroid in the field of a Stokeslet — Equations 13.24, 13.26, 13.29, 13.31, and 13.33 — are consistent with those obtained from the velocity field of a translating spheroid.
Hint: Use of the Lorentz reciprocal theorem.

Exercise 13.2 Error Analysis for Spherical Drops.
Extend the error analysis for rigid spheres (Section 13.3) to the case of the spherical viscous drop. How does the viscosity ratio λ affect the convergence behavior?

Exercise 13.3 Boundary Collocation for the Oblate Spheroid with Lamb's General Solution.
Consider an oblate spheroid in an axisymmetric streaming flow. Expand the velocity with Lamb's general solution and examine the convergence behavior of the collocation solution. At what aspect ratio does the method deteriorate?

Exercise 13.4 Convergence of Torque and Stresslet Coefficients.
Consider a stationary, nonrotating sphere in an ambient field produced by a nearby Stokeslet. Examine the convergence of a_{02}, a_{12}, and c_{11} as a function of the number of collocation points, in a manner analogous to the discussion on a_{01} and a_{11} (see Figure 13.4).
Comment: The analysis of these coefficients reveals the rate at which the torque and stresslet resistance functions converge with number of collocations points.

Exercise 13.5 Collocation Schemes for Two Unequal Spheres.
It seems reasonable that for two unequal spheres, the larger sphere should receive a greater number of collocation points, given that the total number of points $N_1 + N_2$ is fixed. In this problem, we offer additional guidelines for distributing the points between the two spheres. Given spheres sizes and center-to-center separation, examine each sphere in turn, with the other sphere replaced by an "equivalent" Stokeslet. Use the error analysis from the sphere-Stokeslet problem to determine an acceptable value for the number of collocation points.
Hint: Consider the following options for the equivalent Stokeslet:

1. For lubrication-type problems, large stresses develop in the gap region, so the Stokeslet is located at the nearest point on the surface of the other sphere.
2. For surfaces moving in tandem as a rigid body, the gap region does not dominate the flow, so the equivalent Stokeslet is located at the center of the other sphere.

Do these strategies provide optimal rates of convergence?
Note: An example program for the two unequal spheres is available on `flossie`, in the subdirectory `chapter13`. (See the instructions in the preamble of this book for copying computer programs over Internet.)

References

[1] G. K. Batchelor and J. T. Green. The hydrodynamic interaction of two small freely-moving spheres in a linear flow field. *J. Fluid Mech.*, 56:375–400, 1972.

[2] G. K. Batchelor and J. T. Green. The determination of the bulk stress in a suspension of spherical particles to order c^2. *J. Fluid Mech.*, 56:401–427, 1972.

[3] V. N. Beshkov, B.P. Radoev, and I. B. Ivanov. Slow motion of two droplets and a droplet towards a fluid or solid interface. *Intl. J. Multiphase Flow*, 4:563–570, 1978.

[4] H. Brenner. The slow motion of a sphere through a viscous fluid towards a plane surface. *Chem. Eng. Sci.*, 16:242–251, 1961.

[5] H. Brenner and M. E. O'Neill. On the Stokes resistance of multiparticle systems in a linear shear field. *Chem. Eng. Sci.*, 27:1421–1439, 1972.

[6] S. B. Chen and H. J. Keh. Electrophoresis in a dilute suspension of colloidal spheres. *AIChE J.*, 34:1075–1085, 1988.

[7] R. M. Corless and D. J. Jeffrey. Stress moments of nearly touching spheres in low Reynolds number flow. *Z. Angew. Math. Phys.*, 39:874–884, 1988.

[8] R. G. Cox and H. Brenner. The slow motion of a sphere through a viscous fluid towards a plane surface. Part II. Small gap widths, including inertial effects. *Chem. Eng. Sci.*, 22:1753–1777, 1967.

[9] R. G. Cox. The deformation of a drop in a general time-dependent fluid flow. *J. Fluid Mech.*, 37:601–623, 1969.

[10] Z. Dagan, S. Weinbaum, and R. Pfeffer. General theory for the creeping motion of a finite sphere along the axis of a circular orifice. *J. Fluid Mech.*, 117:143–170, 1982.

[11] G. Dahlquist and A. Bjorck. *Numerical Methods.* Prentice-Hall, Englewood Cliffs, 1974. Translated by Ned Anderson.

[12] R. H. Davis, J. A. Schonberg, and J. M. Rallison. The lubrication force between two viscous drops. *Phys. Fluids*, A1:77–81, 1989.

[13] H. Faxén. Der Widerstand gegen die Bewegung einer starren Kugel in einer zähen Flüssigkeit, die zwischen zwei parallelen Ebenen Wänden eingeschlossen ist (The resistance against the movement of a rigid sphere in a viscous fluid enclosed between two parallel planes). *Arkiv fur Matematik, Astronomi och Fysik*, 18(29):1–52, 1924.

[14] D. L. Feke and W. R. Schowalter. The effect of Brownian diffusion on shear-induced coagulation of colloidal dispersion. *J. Fluid Mech.*, 133:17–35, 1983.

[15] D. L. Feke and W. R. Schowalter. The influence of Brownian diffusion on binary flow-induced collision rates in colloidal dispersions. *J. Colloid Interface Sci.*, 106:203–214, 1985.

[16] Y. O. Fuentes, S. Kim, and D. J. Jeffrey. Mobility functions for two unequal viscous drops in Stokes flow I. Axisymmetric motions. *Phys. Fluids*, 31:2445–2455, 1988.

[17] Y. O. Fuentes, S. Kim, and D. J. Jeffrey. Mobility functions for two unequal viscous drops in Stokes flow II. Asymmetric motions. *Phys. Fluids*, A1:61–76, 1989.

[18] P. Ganatos, R. Pfeffer, and S. Weinbaum. A numerical-solution technique for three-dimensional Stokes flows, with application to the motion of strongly interacting spheres in a plane. *J. Fluid Mech.*, 84:79–111, 1978.

[19] P. Ganatos, S. Weinbaum, and R. Pfeffer. A strong interaction theory for the creeping motion of a sphere between plane parallel boundaries. Part 1. Perpendicular motion. *J. Fluid Mech.*, 99:739–753, 1980.

[20] P. Ganatos, R. Pfeffer, and S. Weinbaum. A strong interaction theory for the creeping motion of a sphere between plane parallel boundaries. Part 2. Parallel motion. *J. Fluid Mech.*, 99:755–783, 1980.

[21] M. J. Gluckman, R. Pfeffer, and S. Weinbaum. A new technique for treating multiparticle slow viscous flow: axisymmetric flow past spheres and spheroids. *J. Fluid Mech.*, 50:705–740, 1971.

[22] A. J. Goldman, R. G. Cox, and H. Brenner. Slow viscous motion of a sphere parallel to a plane wall — I. Motion through a quiescent fluid. *Chem. Eng. Sci.*, 22:637–651, 1967.

[23] J. T. Green. *Properties of Suspensions of Rigid Spheres.* Ph. D. Dissertation, University of Cambridge, 1971.

[24] S. Haber, G. Hetsroni, and A. Solan. On the low Reynolds number motion of two droplets. *Intl. J. Multiphase Flow*, 1:57–71, 1973.

[25] W. W. Hackborn. Asymmetric Stokes flow between parallel planes due to a rotlet. *J. Fluid Mech.*, 000:000–000, 1990.

[26] R. E. Hansford. On converging solid spheres in a highly viscous fluid. *Mathematika*, 17:250–254, 1970.

[27] J. Happel and H. Brenner. *Low Reynolds Number Hydrodynamics.* Martinus Nijhoff, The Hague, 1983.

[28] J. J. L. Higdon. A hydrodynamic analysis of flagellar propulsion. *J. Fluid Mech.*, 90:685–711, 1979.

[29] E. J. Hinch. An averaged-equation approach to particle interactions in a fluid suspension. *J. Fluid Mech.*, 83:695–720, 1977.

[30] E. W. Hobson. *The Theory of Spherical and Ellipsoidal Harmonics.* Chelsea, New York, 1955.

[31] R. Hsu and P. Ganatos. The motion of a rigid body in a viscous fluid bounded by a plane wall. *J. Fluid Mech.*, 207:29–72, 1989.

[32] J. N. Israelachvili. The calculation of van der Waals dispersion forces between macroscopic bodies. *Proc. R. Soc.*, A331:39–55, 1972.

[33] J. N. Israelachvili. Van der Waals forces in biological systems. *Q. Rev. Biophys.*, 6:341–387, 1974.

[34] J. N. Israelachvili and B. W. Ninham. Intermolecular forces — the long and short of it. *J. Colloid Interface Sci.*, 58:14–25, 1977.

[35] K. M. Jansons and J. R. Lister. The general solution of Stokes flow in a half-space as an integral of the velocity on the boundary. *Phys. Fluids*, 31:1321–1323, 1988.

[36] D. J. Jeffrey. Group expansions for the bulk properties of a statistically homogeneous, random suspension. *Proc. R. Soc. (London) A*, 338:503–516, 1974.

[37] D. J. Jeffrey. Low-Reynolds-number flow between converging spheres. *Mathematika*, 29:58–66, 1982.

[38] D. J. Jeffrey and Y. Onishi. Calculation of the resistance and mobility functions for two unequal rigid spheres in low-Reynolds-number flow. *J. Fluid Mech.*, 139:261–290, 1984.

[39] D. J. Jeffrey and Y. Onishi. The forces and couples acting on two nearly touching spheres in low-Reynolds-number flow. *Z. Angew. Math. Phys.*, 35:634–641, 1984.

[40] D. J. Jeffrey and R. M. Corless. Forces and stresslets for the axisymmetric motion of nearly touching unequal spheres. *PCH PhysicoChem. Hydrodynamics*, 10:461–470, 1988.

[41] D. J. Jeffrey. Stresslet resistance functions for low Reynolds number flow using deformable spheres. *Z. Angew. Math. Phys.*, 40:1–8, 1989.

[42] H. J. Keh and J. L. Anderson. Boundary effects on electrophoretic motion of colloidal spheres. *J. Fluid Mech.*, 153:417–439, 1985.

[43] S. Kim. *Modeling of Porous Media via Renormalization of the Stokes Equations.* Ph.D. Dissertation, Princeton University, 1983.

[44] S. Kim. Sedimentation of two arbitrarily oriented spheroids in a viscous fluid. *Intl. J. Multiphase Flow*, 11(5):699–712, 1985.

[45] S. Kim and R. T. Mifflin. The resistance and mobility functions of two equal spheres in low-Reynolds-number flow. *Phys. Fluids*, 28:2033–2045, 1985.

[46] S. Kim. Stokes flow past three spheres: an analytic solution. *Phys. Fluids*, 30(8):2309–2314, 1987.

[47] S. H. Lee, R. S. Chadwick, and L. G. Leal. Motion of a sphere in the presence of a plane interface. Part 1. An approximate solution by generalization of the method of Lorentz. *J. Fluid Mech.*, 93:705–726, 1979.

[48] S. H. Lee and L. G. Leal. The motion of a sphere in the presence of a deformable interface II. A numerical study of the translation of a sphere normal to an interface. *J. Colloid Interface Sci.*, 87(1):81–106, 1982.

[49] S. Leichtberg, S. Weinbaum, R. Pfeffer, and M. J. Gluckman. A study of unsteady forces at low Reynolds number: a strong interaction theory for the coaxial settling of three or more spheres. *Phil. Trans. R. Soc. (London)*, A282:585–613, 1976.

[50] W. H. Liao and D. Krueger. Multipole expansion calculation of slow viscous flow about spheroids of different sizes. *J. Fluid Mech.*, 96:223–241, 1980.

[51] N. Liron and S. Mochon. Stokes flow for a Stokeslet between two parallel flat plates. *J. Eng. Math.*, 10:287–303, 1976.

[52] H. A. Lorentz. Ein allgemeiner Satz, die Bewegung einer reibenden Flüssigkeit betreffend, nebst einigen Anwendungen desselben (A general theorem concerning the motion of a viscous fluid and a few applications from it). *Versl. Kon. Akad. Wetensch. Amsterdam*, 5:168–174, 1896. Also in *Abhandlungen über Theoretische Physik*, 1:23–42 (1907) and *Collected Papers*, 4:7–14, Martinus Nijhoff, The Hague, 1937.

[53] S. Y. Lu and S. Kim. The general solution and Faxén laws for the temperature fields in and outside an isolated ellipsoid. *J. Eng. Math.*, 21(3):179–200, 1987.

[54] J. H. C. Luke. Convergence of a multiple reflection method for calculating Stokes flow in a suspension. *SIAM J. Appl. Math.*, 49:1635–1651, 1989.

[55] S. R. Majumdar. Slow motion of an incompressible viscous liquid generated by the rotation of two spheres in contact. *Mathematika*, 14:43–46, 1967.

[56] A. D. Maude. End effects in a falling-sphere viscometer. *Br. J. Appl. Phys.*, 12:293–295, 1961.

[57] R. W. O'Brien. A method for the calculation of the effective transport properties of suspensions of interacting particles. *J. Fluid Mech.*, 91(Part 1):17–39, 1979.

[58] V. O'Brien. Form factors for deformed spheroids in Stokes flow. *AIChE J.*, 14:870–875, 1968.

[59] M. E. O'Neill and K. Stewartson. On the slow motion of a sphere parallel to a nearby wall. *J. Fluid Mech.*, 27:705–724, 1967.

[60] M. E. O'Neill. On asymmetrical slow viscous flows caused by the motion of two equal spheres almost in contact. *Proc. Camb. Phil. Soc.*, 65:543–556, 1969.

[61] M. E. O'Neill and S. R. Majumdar. Asymmetrical slow viscous fluid motions caused by the translation or rotation of two spheres. Part II: Asymptotic forms of the solutions when the minimum clearance between the spheres approaches zero. *Z. Angew. Math. Phys.*, 21:180–187, 1970.

[62] C. W. Oseen. *Hydrodynamik.* Akad. Verlagsgesellschaft, Leipzig, 1927.

[63] O. Pinkus and B. Sternlicht. *Lubrication Theory.* McGraw-Hill, New York, 1961.

[64] M. Smoluchowski. On the mutual action of spheres which move in a viscous liquid. *Bull. Acad. Sci. Cracovie A*, 1:28–39, 1911.

[65] S. Weinbaum, P. Ganatos, and Z. Yan. Numerical multipole and boundary integral equation techniques in Stokes flow. *Ann. Rev. Fluid Mech.*, 22:275–316, 1990.

[66] S. -M. Yang and L. G. Leal. Particle motion in Stokes flow near a plane fluid-fluid interface. Part 1. Slender body in a quiescent fluid. *J. Fluid Mech.*, 136:393–421, 1983.

[67] S. -M. Yang and L. G. Leal. Particle motion in Stokes flow near a plane fluid-fluid interface. Part 1. Linear shear and axisymmetric straining flows. *J. Fluid Mech.*, 149:275–304, 1984.

[68] S. -M. Yang and L. G. Leal. Particle motion in Stokes flow near a deformed fluid-fluid interface. *Intl. J. Multiphase Flow*, 16:597–616, 1990.

[69] B. J. Yoon and S. Kim. Note on the direct calculation of mobility functions for two equal-sized spheres in Stokes flow. *J. Fluid Mech.*, 185:437–446, 1987.

[70] R. H. Yoon and G. H. Luttrell. The effect of bubble size on fine particle flotation. *Mineral Proc. and Extrac. Metall. Rev.*, 5:101–122, 1989.

[71] B. J. Yoon and S. Kim. A boundary collocation method for the motion of two spheroids in Stokes flow: hydrodynamic and colloidal interactions. *Intl. J. Multiphase Flow*, 16:639–650, 1990.

[72] A. Z. Zinchenko. Calculation of hydrodynamic interaction between drops at low Reynolds number. *PMM Applied Math. and Mech.* 42:1046–1051, 1978.

[73] A. Z. Zinchenko. The slow asymmetric motion of two drops in a viscous medium. *PMM Applied Math. and Mech.* 44:30–37, 1981.

[74] A. Z. Zinchenko. Calculation of close interaction between two drops, with internal circulation and slip effect taken into account. *PMM Applied Math. and Mech.* 45:564–567, 1982.

[75] A. Z. Zinchenko. Hydrodynamic interaction of two identical liquid spheres in linear flow field. *PMM Applied Math. and Mech.* 47:37–43, 1984.

[76] A. Z. Zinchenko. Effect of hydrodynamic interactions between the particles on the rheological properties of dilute emulsions. *PMM Applied Math. and Mech.* 48:198–206, 1984.